

# Oxygen diffusion and surface exchange studies on (La<sub>0.75</sub>Sr<sub>0.25</sub>)<sub>0.95</sub>Cr<sub>0.5</sub>Mn<sub>0.5</sub>O<sub>3-δ</sub>

Edwin S. Raj<sup>a,\*</sup>, John A. Kilner<sup>b</sup>, John T.S. Irvine<sup>a</sup>

<sup>a</sup> School of Chemistry, University of St Andrews, Fife KY16 9ST, Scotland, UK

<sup>b</sup> Department of Materials, Imperial College London, London SW7 2BP, UK

Received 1 July 2005; received in revised form 11 April 2006; accepted 13 April 2006

## Abstract

Oxygen tracer diffusion coefficient ( $D^*$ ) and surface exchange coefficient ( $k^*$ ) have been measured for (La<sub>0.75</sub>Sr<sub>0.25</sub>)<sub>0.95</sub>Cr<sub>0.5</sub>Mn<sub>0.5</sub>O<sub>3-δ</sub> using isotopic exchange and depth profiling by secondary ion mass spectrometry technique as a function of temperature (700–1000 °C) in dry oxygen and in a water vapour-forming gas mixture. The typical values of  $D^*$  under oxidising and reducing conditions at ~1000 °C are  $4 \times 10^{-10}$  cm<sup>2</sup> s<sup>-1</sup> and  $3 \times 10^{-8}$  cm<sup>2</sup> s<sup>-1</sup> respectively, whereas the values of  $k^*$  under oxidising and reducing conditions at ~1000 °C are  $5 \times 10^{-8}$  cm s<sup>-1</sup> and  $4 \times 10^{-8}$  cm s<sup>-1</sup> respectively. The apparent activation energies for  $D^*$  in oxidising and reducing conditions are 0.8 eV and 1.9 eV respectively.

© 2006 Elsevier B.V. All rights reserved.

**Keywords:** Oxygen diffusion; Surface exchange; SIMS; IEDP; LSCM

## 1. Introduction

Solid oxide fuel cells (SOFC) offer several advantages over conventional power generation systems, notably the ability to use carbon monoxide as a fuel and the possibility of co-generation with gas turbine power systems to achieve optimal efficiency. Although cost is the notable barrier to widespread SOFC implementation, the most important technical barriers currently being addressed relate to fuel electrode or anode [1]. The conventional anode for the zirconia-based SOFCs are Ni/YSZ cermets, which display excellent catalytic properties for fuel oxidation and current collection [2], however suffer from problems arising from carbon deposition while using hydrocarbon fuels, low tolerance to sulphur and poor redox cycling, causing volume instability. The nickel metal in the cermet also tends to agglomerate during prolonged operation, leading to reduced three-phase boundary and increasing resistance. In order to overcome the disadvantages of the traditional Ni-YSZ cermet anode, alternative oxides are being investigated as potential anodes for SOFCs.

The perovskite oxides, in particular doped LaMnO<sub>3</sub>, are an interesting class of materials for this purpose as they are stable in both oxidative and reductive atmospheres. They can also be substituted on the A and B sites with alkali earth and transition metal elements respectively, which allows interesting modifications of their electronic as well as their catalytic properties. Recently, Tao and Irvine reported a redox stable La<sub>1-x</sub>Sr<sub>x</sub>Cr<sub>1-y</sub>Mn<sub>y</sub>O<sub>3-δ</sub> fuel electrode for SOFCs, with comparable performance to traditional cermet anodes [3]. The introduction of A-site deficiency is thought to decrease the reactivity of perovskite with the electrolyte and several compositions including (La<sub>0.75</sub>Sr<sub>0.25</sub>)<sub>0.95</sub>Cr<sub>0.5</sub>Mn<sub>0.5</sub>O<sub>3-δ</sub> (LSCM) were also investigated and reported [4].

Mass transport through the oxide membrane is determined by the tracer oxygen diffusion coefficient ( $D^*$ ) and surface exchange coefficient ( $k^*$ ). Both  $D^*$  and  $k^*$  are measured by following the movement of a chemically identical tracer atom, <sup>18</sup>O, and the diffusion profile within the sample determined by Secondary Ion Mass Spectrometry (SIMS). This approach known as Isotope Exchange Depth Profile (IEDP) [5] gives accurate values of oxygen diffusion and oxygen surface exchange coefficients and also provides an insight into oxygen flux in ceramics.

Various oxygen diffusion studies give either the chemical diffusion coefficient or the tracer diffusion coefficient. Tracer

\* Corresponding author.

E-mail address: [esr1@st-andrews.ac.uk](mailto:esr1@st-andrews.ac.uk) (E.S. Raj).

Table 1  
Experimental conditions

| (a) $D^*$ and $k^*$ for samples exchanged in dry $^{18}\text{O}_2$ at $\sim 0.2$ atm                                  |                         |              |   |                              |                                       |                              |       |        |
|---|-------------------------|--------------|---|------------------------------|---------------------------------------|------------------------------|-------|--------|
| Exchange temperature ( $^{\circ}\text{C}$ )   | Exchange pressure (atm) | $t_{18}$ (h) | $D^*$ ( $\text{cm}^2 \text{s}^{-1}$ )         | $k^*$ ( $\text{cm s}^{-1}$ ) | $C_o$                                 | $\eta$                       |       |        |
| 716   | 0.21                    | 3            | $6.98 \times 10^{-11}$                        | $3.64 \times 10^{-10}$       | 0.0035                                | 0.005                        |       |        |
| 814   | 0.23                    | 3            | $1.67 \times 10^{-10}$                        | $1.72 \times 10^{-9}$        | 0.02                                  | 0.014                        |       |        |
| 912   | 0.23                    | 3            | $1.10 \times 10^{-10}$                        | $9.74 \times 10^{-9}$        | 0.12                                  | 0.096                        |       |        |
| 1010  | 0.23                    | 3            | $4.74 \times 10^{-10}$                        | $5.49 \times 10^{-8}$        | 0.29                                  | 0.260                        |       |        |
| (b) $D^*$ and $k^*$ for samples exchanged in $\text{H}_2^{18}\text{O}$ –10% $\text{H}_2/\text{N}_2$ at $\sim 0.4$ atm |                         |              |   |                              |                                       |                              |       |        |
| Exchange temperature ( $^{\circ}\text{C}$ )   | Exchange pressure (atm) | $t_{18}$ (h) | Water bath temperature ( $^{\circ}\text{C}$ ) | $\text{Po}_2$ (atm)          | $D^*$ ( $\text{cm}^2 \text{s}^{-1}$ ) | $k^*$ ( $\text{cm s}^{-1}$ ) | $C_o$ | $\eta$ |
| 702   | 0.42                    | 3            | 47.3  | $1.02 \times 10^{-21}$       | $8.69 \times 10^{-10}$                | $5.87 \times 10^{-8}$        | 0.12  | 0.205  |
| 778   | 0.43                    | 3            | 47.8  | $7.63 \times 10^{-20}$       | $1.14 \times 10^{-9}$                 | $3.71 \times 10^{-7}$        | 0.57  | 1.142  |
| 849   | 0.38                    | 3            | 47.7  | $2.53 \times 10^{-18}$       | $3.40 \times 10^{-9}$                 | $3.60 \times 10^{-7}$        | 0.43  | 0.642  |
| 895   | 0.44                    | 3            | 49.4  | $1.95 \times 10^{-17}$       | $1.95 \times 10^{-8}$                 | $9.20 \times 10^{-8}$        | 0.08  | 0.026  |
| 975   | 0.38                    | 3            | 47.4  | $4.75 \times 10^{-16}$       | $3.79 \times 10^{-8}$                 | $4.56 \times 10^{-8}$        | 0.03  | 0.020  |

$C_o$  is the normalized  $^{18}\text{O}$  concentration and  $\eta$  is calculated from Eq. (3).

diffusion coefficient measures the rate of diffusion at equilibrium and in the absence of chemical potential whereas chemical diffusion is due to the simultaneous motion of different types of charged defects in order to maintain electroneutrality, the latter is usually much greater than  $D^*$  for the same composition and temperature [6]. The measurement of the tracer diffusion coefficient is now widely used because of the high level of inaccuracy that may be encountered in most experimental methods used to determine the chemical diffusion coefficient. In this study, the oxygen tracer diffusion coefficient in  $(\text{La}_{0.75}\text{Sr}_{0.25})_{0.95}\text{Cr}_{0.5}\text{Mn}_{0.5}\text{O}_{3-\delta}$ , under oxidising and reducing atmospheres, are investigated.

## 2. Experimental

LSCM was prepared by conventional high temperature solid state route. The starting materials were  $\text{La}_2\text{O}_3$ ,  $\text{SrCO}_3$ ,  $\text{Cr}_2\text{O}_3$  and

$\text{Mn}_2\text{O}_3$ , which were fired at around  $1200\text{ }^{\circ}\text{C}$  with intermediate grindings until a single-phase perovskite was obtained. The phase purity was ascertained before and after exchanges from powder diffraction patterns recorded on a Philips PW1720 diffractometer. The as-synthesized powders were ball milled in acetone, cold-isopressed at 300 MPa and sintered at  $1475\text{ }^{\circ}\text{C}$  to yield dense pellets of relative density greater than 98%, thus ensuring gas tightness. Several pellets of similar dimensions were mounted on a copper block using a low melting wax, carefully abraded with 1200 grade silicon carbide paper and then polished with successive grades of diamond suspension to a  $0.25\text{ }\mu\text{m}$  mirror finish. The polished samples were then demounted, ultrasonically cleaned with acetone and deionised water and dried in a hot oven.

The diffusion apparatus used for exchange in dry oxygen is described elsewhere [5]. Exchanges under wet conditions involved attaching a glass-finger containing normal or isotope enriched water, housed in a water bath. The samples were equilibrated in

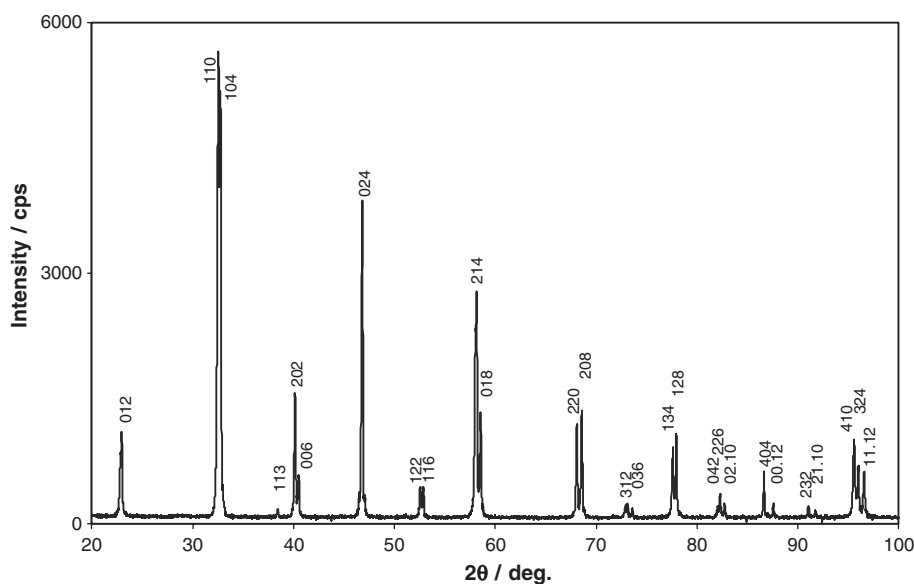


Fig. 1. XRD pattern of  $(\text{La}_{0.75}\text{Sr}_{0.25})_{0.95}\text{Cr}_{0.5}\text{Mn}_{0.5}\text{O}_{3-\delta}$  obtained after exchanging at  $1000\text{ }^{\circ}\text{C}$  in  $\text{H}_2^{18}\text{O}$ /forming gas for  $\sim 15$  h (asterisk indicates vaseline peak).

research grade normal isotopic abundant  $^{16}\text{O}_2$  or 12%  $\text{H}_2^{16}\text{O}$ –9%  $\text{H}_2/79\% \text{N}_2$  for about 12 h, at the same temperature of the intended tracer anneal. After each preannealing, the research grade gas was removed and either  $^{18}\text{O}_2$  (Isotec, USA) or  $\text{H}_2^{18}\text{O}$  ( $^{18}\text{O}$ , Isotec, USA)/10%  $\text{H}_2/\text{N}_2$  (BOC) was introduced. The samples were rapidly heated to the target temperature, annealed and rapidly cooled. The sample temperature was monitored by a Pt/Rh thermocouple situated at the close proximity of the sample. The isotopic anneal time was calculated from the temperature–time profile.

The  $^{18}\text{O}$  penetration profiles of the annealed samples were determined by SIMS in an Atomika 6500 Ion Microprobe. The detailed SIMS analysis procedure can be found elsewhere [7]. For line scans, the exchanged samples were cut perpendicular to the exchanged face, the cross section mirror-polished and placed normal to the focused ion beam. Since the tracer concentration reached background level at the centre of all specimens, the solution to diffusion equation (1) involving only one surface (semi-infinite solid) was used [8]:

$$C_1(x) = \frac{C(x) - C_{\text{bg}}}{C_{\text{g}} - C_{\text{bg}}} = \text{erfc}\left(\frac{x}{2\sqrt{D^*t}}\right) - e^{(hx + h^2D^*t)} \text{erfc}\left\{\left(\frac{x}{2\sqrt{D^*t}}\right) + (h\sqrt{D^*t})\right\} \quad (1)$$

where  $C_1(x)$  is normalized  $^{18}\text{O}$  concentration corrected for the natural isotopic background,  $C(x)$  is  $^{18}\text{O}$  concentration,  $C_{\text{bg}}$  is background concentration,  $C_{\text{g}}$  is gas concentration,  $h = k^*/D^*$ ,  $t$  is the time of the  $^{18}\text{O}_2$  anneal and  $\text{erfc}$  is the complementary error function.

### 3. Results and discussion

The LSCM sample was single-phase as identified from XRD. Isotopic exchanges were carried out both in air and reducing

ambient ( $P_{\text{O}_2}$  values are listed in Table 1(b)); hence the single-phase nature of LSCM exchanged at 10%  $\text{H}_2/\text{N}_2$  at 1000 °C was examined by XRD. The XRD shows no indication of either a phase change or decomposition even after exchanging at very low oxygen partial pressures for several hours, which is reproduced in Fig. 1. The calculated cell parameters after exchanging in reducing conditions that correspond to  $R\text{-}3c$  space group are:  $a = 5.5070(9)$  Å,  $c = 13.3640(1)$  Å and volume =  $350.99(1)$  Å<sup>3</sup>. This unit cell volume is consistent with the data previously reported for LSCM reduction under slightly dry conditions [4].

Oxygen diffusivity has been shown to be directly proportional to the concentration of oxygen vacancies [9]. The surface exchange rate constant, on the other hand, can be a limiting factor for the overall transport of oxygen through thin membranes [10]. For exchange from oxygen molecules close to 1 atm, it was found that  $k^*$  increases with bulk concentration of oxygen vacancies and on the basis of which it has been proposed that oxygen incorporation involves an oxygen vacancy at the surface of the oxide [11].

The true  $^{18}\text{O}$  background in the specimens ( $C_{\text{bg}}$ ) was calculated from the depth profiles of the unexchanged specimen to be 0.213%. The  $^{18}\text{O}$  fraction of total oxygen atoms in the gas phase ( $C_{\text{g}}$ ) during the isotopic anneal was calculated by the oxidation of silicon single crystals to silicon dioxide in the same atmosphere, followed by SIMS analysis. For  $^{18}\text{O}_2$  ambient,  $C_{\text{g}}$  was 22% and for  $\text{H}_2^{18}\text{O}$ ,  $C_{\text{g}}$  was calculated to be 42%. Isotopic exchanges were carried out in the temperature range of 700–1000 °C in (i)  $^{18}\text{O}_2$  and (ii) 12%  $\text{H}_2^{18}\text{O}$ –9%  $\text{H}_2/79\% \text{N}_2$ . The cross section of LSCM obtained after exchanging at different temperatures and ambient were analysed in an SEM which indicated the absence of any surface cracks, apart from few grains being knocked out during polishing and might contribute to localised variations in the surface  $^{18}\text{O}$  fraction.

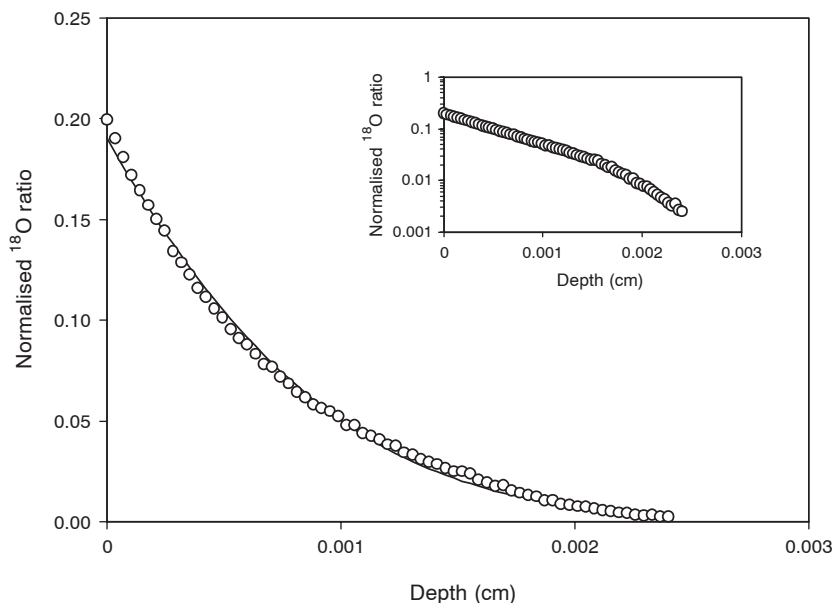


Fig. 2.  $^{18}\text{O}$  penetration profile of  $(\text{La}_{0.75}\text{Sr}_{0.25})_{0.95}\text{Cr}_{0.5}\text{Mn}_{0.5}\text{O}_{3-\delta}$  measured by SIMS line scan after exchanging at 650 °C in  $^{18}\text{O}_2$  for 3 h (circles indicate the experimental data and line indicates the best fit).

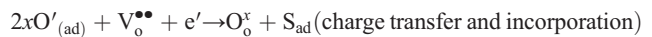
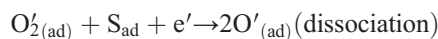
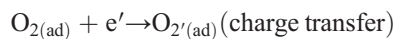
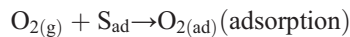
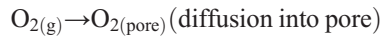
A typical  $^{18}\text{O}$  diffusion profile obtained by line scan along the cross section and the corresponding theoretical fit of LSCM is given in Fig. 2. A good agreement between the experimental data and theoretical fit can be observed. The inset is the normalized  $^{18}\text{O}$  fraction on a log scale. Some deviation in the fit, especially at low tracer concentration was observed, which may be due to several reasons including tracer concentration not reaching background level at the centre, faster diffusion along dislocations and grain boundaries, as well as errors due to subtraction of natural isotopic abundance [12], hence, these data points were ignored while calculating  $D^*$  and  $k^*$ . An apparent drop in the  $^{18}\text{O}$  concentration closer to the surface was observed and is attributed to the artefact caused by the lateral resolution of ion beam (6–12  $\mu\text{m}$ ) as it crosses the edge of the specimen. Ideally, the first data point should correspond to the true surface concentration however, some anomalies in the  $^{18}\text{O}$  fraction were observed and in such cases, the steady state value was taken as the true surface concentration. A tailing effect was observed for LSCM exchanged at 1000  $^\circ\text{C}$  in  $\text{H}_2^{18}\text{O}/\text{H}_2$  only which is usually taken as the evidence for fast or short-circuit diffusion resulting from extended defects such as grain boundaries and dislocations [13].

The oxygen exchange parameters for LSCM exchanged in dry  $^{18}\text{O}_2$  and  $\text{H}_2^{18}\text{O}-10\% \text{H}_2/\text{N}_2$  are given in Table 1(a) and (b). The Arrhenius plots of both  $D^*$  and  $k^*$  as a function of temperature are given in Fig. 3(a) and (b). The plotted error bars are the estimated standard deviations for  $D^*$  and  $k^*$ . Under dry  $^{18}\text{O}_2$  conditions, both  $D^*$  and  $k^*$  show linear increase with increasing temperature (700 to 1000  $^\circ\text{C}$ ), but  $k^*$  increases more rapidly than  $D^*$ . Under wet reducing conditions,  $D^*$  tends to a near linear increase with increasing temperature in the Arrhenius plot although a large scatter in  $k^*$  was observed (Fig. 3(b)). Both values are significantly higher than under oxidising conditions. This is in agreement with the studies carried out under reducing conditions on oxides including  $\text{La}_{1-x}\text{Sr}_x\text{Fe}_{1-y}\text{Co}_y\text{O}_{3-\delta}$  [14],  $\text{M}_{1-x}\text{Y}_x\text{O}_{2-x}$  ( $\text{M}=\text{Zr}, \text{Ce}$ ) [15] where an increase in  $k^*$  was reported with decreasing oxygen activity. The high values of  $k^*$  even in reducing atmospheres indicates that exchange with oxygen in the  $\text{H}_2\text{O}$  molecule occurs at a similar rate to that with  $\text{O}_2$  molecule under oxidising conditions at high temperatures or perhaps even faster. Thermogravimetric studies on  $\text{La}_{0.75}\text{Sr}_{0.25}\text{Mn}_{0.5}\text{Cr}_{0.5}\text{O}_3$  indicate that it transforms to approximately  $\text{La}_{0.75}\text{Sr}_{0.25}\text{Mn}_{0.5}\text{Cr}_{0.5}\text{O}_{2.75}$  under reducing conditions [4], similar to the forming gas used in the exchange studies here. Thus, the difference in the oxygen vacancy content between the oxidising and reducing atmospheres, with more ionic carriers under reducing conditions, justifies the enhanced diffusion coefficient in forming gas.

The near linear increase with increasing temperature allows Arrhenius parameters to be calculated, except for  $k^*$  in reducing atmospheres, where there is scatter similar to that previously observed for LSCF in wet reducing conditions [12]. It should be mentioned that the line scan limitations [7] have been considered during the SIMS measurements and they are probably not the origin of the scattering of data. As seen from Table 2, the activation energy for diffusion coefficient in reducing conditions (1.9 eV) is more than twice that of  $D^*$  under oxidising conditions (0.8 eV), although the observed value for  $D^*$  is much higher for the former. The activation energy for surface exchange coefficient

under oxidising conditions is quite high (2.4 eV) in comparison with similar systems reported in the literature and summarised in Table 2. The activation energy for  $D^*$  under oxidising conditions is consistent with noninteracting vacancies. However, the corresponding activation energy under reducing conditions is unusually high which suggests greater defect association or short-range ordering or could also be due to the change in vacancy concentration with temperature due to reduction and changes in  $P_{\text{O}_2}$ , thus increasing the activation energy.

Generally, the dissociation of molecular oxygen requires charge transfer and may involve a number of possible steps [21]



The high activation energy for  $k^*$  under oxidising conditions (2.39 eV) may be due to the fact that the dissociation of oxygen is slow in relation to the bulk incorporation [19]. The dissociation

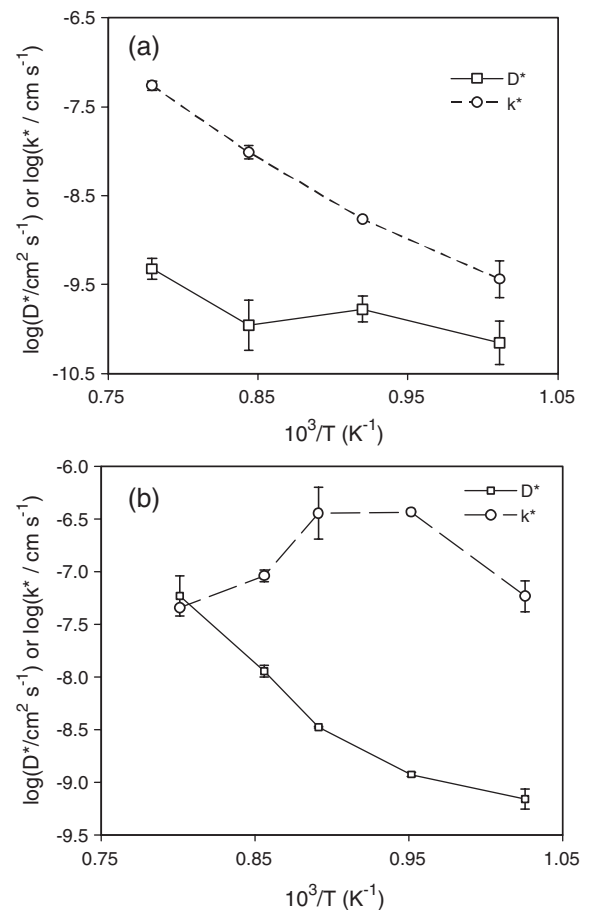


Fig. 3. Arrhenius plot of  $D^*$  and  $k^*$  of  $(\text{La}_{0.75}\text{Sr}_{0.25})_{0.95}\text{Cr}_{0.5}\text{Mn}_{0.5}\text{O}_{3-\delta}$  exchanged in (a) dry  $^{18}\text{O}_2$  and (b)  $\text{H}_2^{18}\text{O}/\text{forming gas}$ , in the temperature range of 700–1000  $^\circ\text{C}$ . Note: the lines are added to link the data and have no theoretical significance.

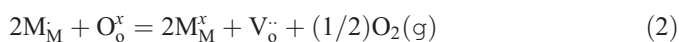
Table 2  
Summary of  $D^*$  and  $k^*$  and Arrhenius parameters (valid in the temperature range of 700–1000 °C) for LSCM and some relevant oxides

| Material   | Atmosphere                                  | $D^*$ (cm <sup>2</sup> s <sup>-1</sup> ) at 900 °C | $E_{D^*}$ (eV) | $k^*$ (cm s <sup>-1</sup> ) at 900 °C | $E_{k^*}$ (eV) | Ref.       |
|--|---|--|----------------|---------------------------------------|----------------|------------|
| LSCM   | <sup>18</sup> O <sub>2</sub>                | $1.0 \times 10^{-10}$                              | 0.8            | $9.7 \times 10^{-9}$                  | 2.4            | This work  |
|  | H <sub>2</sub> <sup>18</sup> O/forming gas  | $1.3 \times 10^{-8}$                               | 1.9            | $9.2 \times 10^{-8}$                  | –              |            |
| La <sub>0.8</sub> Sr <sub>0.2</sub> Cr <sub>0.2</sub> Fe <sub>0.8</sub> O <sub>3-δ</sub> | <sup>18</sup> O <sub>2</sub>                | $9.6 \times 10^{-10}$                              | 2.13           | $3.3 \times 10^{-7}$                  | 1.39           | [12,16,12] |
|  | H <sub>2</sub> <sup>18</sup> O/forming gas  | $2.3 \times 10^{-7}$                               | 0.71           | $6.6 \times 10^{-6}$                  | –              |            |
| La <sub>0.8</sub> Sr <sub>0.2</sub> Co <sub>0.2</sub> Mn <sub>0.8</sub> O <sub>3-δ</sub> | <sup>18</sup> O <sub>2</sub>                | $1.0 \times 10^{-11}$                              | 3.20           | $2.0 \times 10^{-7}$                  | –              | [20]       |
| La <sub>0.8</sub> Sr <sub>0.2</sub> MnO <sub>3+δ</sub>                                   | <sup>18</sup> O <sub>2</sub>                | $3.2 \times 10^{-13}$                              | 2.79           | $1.0 \times 10^{-8}$                  | 1.33           | [17]       |
| YSZ (9.5 mol%) <sup>a</sup>  | <sup>18</sup> O <sub>2</sub>                | $1.0 \times 10^{-7}$                               | 0.8            | $3.0 \times 10^{-6}$                  | 2.2            | [18]       |
| Ce <sub>0.9</sub> Gd <sub>0.1</sub> O <sub>2-x</sub>                                     | <sup>18</sup> O <sub>2</sub> , $T > 700$ °C | $8.0 \times 10^{-8}$                               | 0.9            | $1.0 \times 10^{-6}$                  | 3.3            | [19]       |
|  | $T < 700$ °C                                | –  | –              | –                                     | 0.9            |            |

<sup>a</sup> Single crystal.

of molecular oxygen requires charge transfer, which implies that the availability of free electrons required for charge transfer is the rate-limiting step for oxygen surface exchange.

The oxygen exchange coefficients for La<sub>0.65</sub>Sr<sub>0.35</sub>MnO<sub>3-δ</sub> and La<sub>0.5</sub>Sr<sub>0.5</sub>MnO<sub>3-δ</sub> (LSM) measured in dry oxygen close to 1 atm, are reported in the literature [20]. At 900 °C, the  $D^*$  for La<sub>0.65</sub>Sr<sub>0.35</sub>MnO<sub>3-δ</sub> and La<sub>0.5</sub>Sr<sub>0.5</sub>MnO<sub>3-δ</sub> are  $3 \times 10^{-13}$  cm<sup>2</sup> s<sup>-1</sup> and  $2 \times 10^{-11}$  cm<sup>2</sup> s<sup>-1</sup> respectively.  $k^*$  for the same materials at the same temperature are  $4 \times 10^{-7}$  cm s<sup>-1</sup> and  $9 \times 10^{-7}$  cm s<sup>-1</sup> respectively. In comparison with the  $D^*$  and  $k^*$  values of LSCM calculated from dry oxygen exchanges, it can be seen that the  $D^*$  of LSCM is about 2 orders of magnitude higher but  $k^*$  is about 2 orders of magnitude lower than LSM reported in Ref. [20]. LSCM exchanged in reducing conditions in the present study show an approximately 2 orders of magnitude increase in  $D^*$  at higher temperatures, than those exchanged in oxidising conditions with  $k^*$  also being higher than for (La, Sr)MnO<sub>3-δ</sub>. In LSCM, substitution of Sr onto the ‘A’ site results in a charge compensating transition of Cr<sup>3+</sup>/Mn<sup>3+</sup> to Cr<sup>3+</sup>/Mn<sup>4+</sup> as identified from EXAFS studies [22]. At low  $P_{O_2}$ , charge compensation is achieved by the formation of vacancies, according to Eq. (2):



where M=Mn. This implies that the concentration of oxygen vacancies will increase under reducing conditions, hence an increase in oxide ion conductivity, as is the case in the present

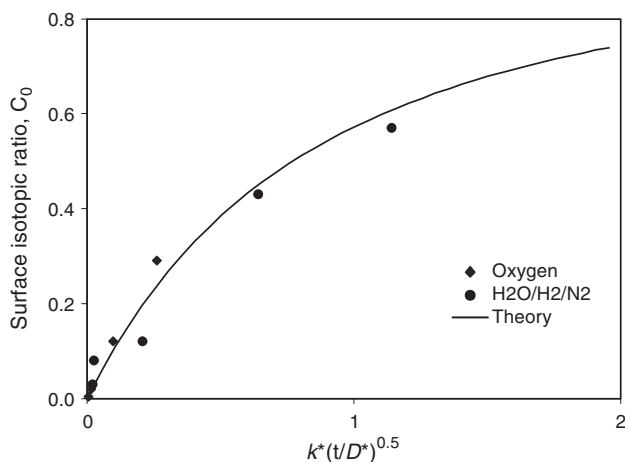


Fig. 4. The normalized surface isotopic fraction,  $C_o$ , of (La<sub>0.75</sub>Sr<sub>0.25</sub>)<sub>0.95</sub>Cr<sub>0.5</sub>Mn<sub>0.5</sub>O<sub>3-δ</sub> as a function of  $\eta$  in oxidising and reducing ambient.

study. This in turn will benefit the ionic transfer and electrochemical reactions at the anode.

Table 1(a) and (b) also give the measured normalized surface <sup>18</sup>O concentration ( $C_o$ ) and the values of  $\eta$  (a dimensionless parameter) calculated using Eq. (3):

$$\eta = k^*(t/D^*)^{0.5} \quad (3)$$

When diffusion occurs into a semi-infinite medium, as is the case of the present study,  $C_o$  and  $\eta$  are related using Eq. (4):

$$C_o = 1 - \exp(-\eta^2) \operatorname{erfc}(\eta) \quad (4)$$

If  $C_o$  is close to 1 and  $\eta > 10$ , the surface exchange is fast compared to diffusion and confidence in  $D^*$  is high, but the confidence in  $k^*$  is low. Conversely, if  $C_o < 1$  and  $\eta < 0.1$ , then the confidence in  $D^*$  decreases due to poor counting statistics as the surface exchange rate slows down [14]. The  $\eta$  values substituted in Eq. (4) gives the theoretical values for  $C_o$ , which are fitted alongside the experimental  $C_o$  values in Fig. 4. This validation plot of  $D^*$  and  $k^*$  clearly demonstrates that all the obtained profiles are consistent.

#### 4. Conclusions

Isotopic exchanges carried out on LSCM under dry <sup>18</sup>O<sub>2</sub> indicates that  $D^*$  for oxygen diffusion gradually increases with increasing temperature, being consistent with the fact that oxygen vacancies are the mobile point defects responsible for oxygen transport. The surface exchange coefficient  $k^*$  increases rapidly with increasing temperature suggesting that lattice oxygen vacancies are involved in the oxygen exchange at the oxide surface. When the oxygen activity is lowered,  $D^*$  increases significantly with temperature whereas the behaviour of  $k^*$  does not seem to be thermally activated, perhaps reflecting the interplay of gas molecules, point defects and electronic charge carriers.  $D^*$  for LSCM is higher than those reported for La<sub>1-x</sub>Sr<sub>x</sub>MnO<sub>3-δ</sub>, however  $k^*$  is lower, which warrants further investigation into ‘A’ and ‘B’ site composition for fine tuning of  $k^*$ . The high activation energy observed for  $D^*$  for reduced LSCM may well indicate some degree of short-range vacancy ordering in this phase. Such ordering would entail an energy penalty for each ion/vacancy hop through the lattice. Although the number of carriers is considerably lower in oxidised LSCM, considerably decreasing the magnitude of  $D^*$ , there will too few vacancies to have any degree

of short-range order. Compared to other manganite and ferrite perovskites (Table 2), the observed values of activation energy are quite typical for  $D^*$ . It may be that these two activation energies reflect regions where vacancy content varies rapidly i.e. as  $(P_{O_2})^{1/4}$  or when these are independent of  $P_{O_2}$ .

### Acknowledgements

Funding from the Carbon Trust and EPSRC including the Supergen Fuel Cells project for this work is gratefully acknowledged. The authors also wish to thank Mr. N. Joomun, Department of Materials, Imperial College London for his assistance during IEDP experiments.

### References

- [1] A. Atkinson, S. Barnett, R.J. Gorte, J.T.S. Irvine, A.J. Mcevoy, M. Mogensen, S.C. Singhal, J. Vohs, Nat. Matters 3 (2004) 17.
- [2] N.Q. Minh, J. Am. Ceram. Soc. 76 (1993) 563.
- [3] S. Tao, J.T.S. Irvine, Nat. Matters 2 (2003) 320.
- [4] S. Tao, J.T.S. Irvine, J. Electrochem. Soc. 151 (2004) A252.
- [5] R.J. Chater, S. Carter, J.A. Kilner, B.C.H. Steele, Solid State Ionics 53–56 (1992) 859.
- [6] J. Maier, Solid State Ionics 112 (1998) 197.
- [7] R.A. DeSouza, J.A. Kilner, Solid State Ionics 106 (1998) 175.
- [8] J. Crank, Mathematics of Diffusion, 2nd edition, Oxford University Press, Oxford, 1975, p. 36.
- [9] T. Ishikagi, S. Yamauchi, K. Kishio, J. Mizusaki, K. Fueki, J. Solid State Chem. 73 (1988) 179.
- [10] B.C.H. Steele, Mater. Sci. Eng., B, Solid-State Mater. Adv. Technol. 13 (1992) 25.
- [11] R.H.E. van Doorn, I.C. Fullarton, R.A. De Souza, J.A. Kilner, H.J.M. Bouwmeester, A.J. Burggraaf, Solid State Ionics 96 (1997) 1.
- [12] A. Atkinson, R.J. Chater, R. Rudkin, Solid State Ionics 139 (2001) 233.
- [13] A.D. Le Claire, A. Rabionovitch, J. Phys. Chem. 14 (1981) 3863.
- [14] S.J. Benson, D. Waller, J.A. Kilner, J. Electrochem Soc. 146 (1999) 1305.
- [15] T. Horita, K. Yamaji, N. Sakai, M. Ishikawa, H. Yokokawa, T. Kawada, M. Dokiya, Electrochem. Solid-State Lett. 1 (1998) 4.
- [16] T. Ramos, A. Atkinson, Solid State Ionics 170 (2004) 275.
- [17] R.A. Desouza, J.A. Kilner, J.F. Walker, Mater. Lett. 43 (2000) 43.
- [18] P.S. Manning, J.D. Sirman, R.A. Desouza, J.A. Kilner, Solid State Ionics 100 (1997) 1.
- [19] P.S. Manning, J.D. Sirman, J.A. Kilner, Solid State Ionics 93 (1997) 125.
- [20] S. Carter, A. Selcuk, R.J. Chater, J. Kajda, J.A. Kilner, B.C.H. Steele, Solid State Ionics 53–56 (1992) 597.
- [21] B.A. Boukamp, B.A. van Hassel, I.C. Vinke, K.J. de Vries, A.J. Burggraaf, Electrochim. Acta 38 (1993) 1817.
- [22] S.M. Plint, P.A. Connor, S. Tao, J.T.S. Irvine, Solid State Ionics 177 (2006) 2005–2008. doi:10.1016/j.ssi.2006.02.025 (this issue).